ADVANCING EARTH AND SPACE SCIENCES

Geophysical Research Letters

RESEARCH LETTER
10.1029/2026GL123624

Diurnal Pulses in Tropical Cyclones as Convectively Coupled Gravity Waves

Katharina Schmitt[1,2], James Ruppert[2], Naoko Sakaeda[2], and Raphaela Vogel[1]

[1]Department of Earth System Sciences—Meteorology, Universität Hamburg, Hamburg, Germany, [2]School of Meteorology, University of Oklahoma, Norman, OK, USA

Key Points:

- Tropical cyclone diurnal pulses are successfully simulated, showing column-spanning signatures consistent with observations
- Diurnal pulses propagate broadly consistent with classical gravity-wave theory, with small deviations likely driven by latent heating
- Diurnal pulses are more frequent at night, likely due to constructive interference with the cyclone's diurnal circulation

Supporting Information:

Supporting Information may be found in the online version of this article.

Correspondence to:

K. Schmitt,
katharina.schmitt@mpimet.mpg.de

Citation:

Schmitt, K., Ruppert, J., Sakaeda, N., & Vogel, R. (2026). Diurnal pulses in tropical cyclones as convectively coupled gravity waves. *Geophysical Research Letters*, *53*, e2026GL123624. https://doi.org/10.1029/2026GL123624

Received 16 APR 2026
Accepted 28 JUL 2026

Author Contributions:

Conceptualization: Katharina Schmitt, James Ruppert, Naoko Sakaeda
Formal analysis: Katharina Schmitt
Funding acquisition: James Ruppert, Raphaela Vogel
Investigation: Katharina Schmitt
Methodology: Katharina Schmitt, James Ruppert, Naoko Sakaeda
Project administration: Katharina Schmitt, James Ruppert
Resources: Katharina Schmitt, James Ruppert
Supervision: James Ruppert, Naoko Sakaeda, Raphaela Vogel

Abstract

This study uses convection-permitting simulations to examine the vertical extent, propagation, and nighttime preference of diurnal pulses (DPs) in tropical cyclones (TCs). DPs are outward-moving rings of cooler brightness temperatures near the storm center and may indicate TC intensification. Their initiation and propagation are poorly understood due to limited high-resolution observations. Here we leverage ensemble case study simulations of Typhoon Haiyan (2013) and Hurricane Maria (2017) to analyze DP events and quantify their structure and propagation characteristics. Results show that DPs are deep, column-spanning features visible in multiple atmospheric variables, including precipitation, temperature, vertical velocity, and radial wind. Interpreted through gravity-wave theory, their speeds and vertical structure largely match theoretical expectations, with deviations that are consistent with convectively coupled gravity waves. DPs are more frequent at night, likely due to constructive interference with the TC's diurnal circulation. These insights into DPs help clarify their initiation and propagation mechanisms.

Plain Language Summary

Diurnal pulses (DPs) are rings of clouds that move outward from the center of tropical cyclones (TCs) as visualized by satellites. They occur on about half of all TC days and in storms of all strengths. Furthermore, their occurrence may be a sign that a storm is getting stronger. Their causes and behavior are not well understood because detailed three-dimensional observations inside these storms are rare. In this study, we used high-resolution numerical model simulations to examine how DPs form and move and why they occur more frequently at night. Our results help paint a three-dimensional picture of DPs that is impossible from satellites alone, showing how they influence rain, temperature, and air motions. We use this new view to examine prior theories for their existence, finding that they are consistent with gravity waves. DPs tend to start at night, possibly due to interactions with the storm's daily circulation cycle.

1. Introduction

Despite substantial advances in understanding tropical cyclone (TC) dynamics, forecasting TC intensity evolution remains challenging, largely due to the complex interactions between environmental conditions and internal storm-scale processes (Cangialosi et al., 2020; Kaplan et al., 2010; Shimada et al., 2018; X. Zhang et al., 2023). One storm-scale phenomenon that may serve as an indicator of intensification, particularly rapid intensification, and can enhance model forecast skill is the diurnal pulse (DP) (X. Zhang & Xu, 2021; X. Zhang et al., 2026). DPs are defined as rings of localized brightness temperature cooling that propagate outward from the storm center (Dunion et al., 2014). Recent studies have shown that DPs occur on approximately 52% of TC days and have been documented across the full spectrum of TC intensity, from tropical storms to major hurricanes (Ditchek et al., 2019; X. Zhang et al., 2023). However, the mechanisms behind their initiation and propagation remain poorly understood, largely due to the lack of high-resolution, three-dimensional observations within TCs.

This study targets specific aspects of initiation and propagation processes by addressing the following key gaps in our understanding:

(i) *Vertical structure of DPs*: To date, DPs have primarily been identified using satellite observations of brightness temperature anomalies. However, X. Zhang and Xu (2022) found that approximately 50% of DPs are associated with precipitation. In addition, Dunion et al. (2019) and Ditchek et al. (2020) further reported DPs exhibiting squall-line characteristics, suggesting that DPs may represent vertically extended structures rather than features confined to the cirrus canopy. However, their full structure remains poorly understood.
(ii) *Timing of their preferential occurrence*: DPs were originally defined not only by brightness temperature anomalies but also by a highly regular "diurnal clock" behavior with initiation typically occurring between

Writing – original draft: Katharina Schmitt
Writing – review & editing: Katharina Schmitt, James Ruppert, Naoko Sakaeda, Raphaela Vogel

00:00 and 04:00 local solar time (LST) and outward propagation reaching radii of approximately 200 km by 04:00–08:00 LST (Dunion et al., 2014). This definition has been challenged by several studies (Trabing & Bell, 2021; X. Zhang et al., 2023), although a moderate global preference for nighttime initiation remains (X. Zhang et al., 2023). The mechanism behind this preference is not yet understood.

(iii) *Propagation mechanism*: The propagation mechanism of DPs remains a topic of debate. Some studies suggest a squall-line-driven process (Ditchek et al., 2020; Dunion et al., 2019), while others propose internal gravity waves as the primary driver (Ditchek et al., 2019; Dunion et al., 2014; Evans & Nolan, 2019; Ruppert & O'Neill, 2019; J. Zhang & Du, 2025; X. Zhang et al., 2023). The gravity wave hypothesis has received greater attention, but most supporting evidence remains indirect, relying on the agreement between observed DP propagation speeds and theoretical gravity wave speeds in the relevant environment (Dunion et al., 2014; X. Zhang et al., 2023), as well as the observed dependence of DP frequency on latitude (J. Zhang & Du, 2025). However, these two propagation mechanisms do not have to be mutually exclusive and could act in combination or transition into one another.

These key gaps are addressed through a case study of two TCs using convection-permitting ensemble simulations with the Weather Research and Forecasting (WRF) model under a realistic physics configuration. We explore three-dimensional anomaly fields during DP events to identify their structure and assess their interaction with the diurnal evolution of the TC circulation, with the aim of explaining their preferential nighttime occurrence. In addition, we provide more direct evidence for the propagation mechanism by examining theoretical propagation angles and phase relationships among relevant variables, in accordance with dry gravity wave theory.

2. Data and Methods

2.1. Weather Research and Forecasting (WRF) Model Simulations

The TCs analyzed in this study are Supertyphoon Haiyan (2013) and Hurricane Maria (2017), both reaching Category 5 intensity. These storms were selected for the modeling experiments as representative cases developing in typical TC genesis environments, characterized by medium vertical wind shear of 6 ms^{-1} for Haiyan (5 ms^{-1} for Maria) and high sea surface temperatures of 29°C for both cases (Razin et al., 2023a, 2023b). These and similar WRF model case study frameworks are described in several prior studies (Luschen & Ruppert, 2024; Luschen et al., 2026; Ruppert et al., 2020).

Both case studies consist of 10-member ensemble simulations conducted using the Advanced Research Weather Research and Forecasting model (WRF-ARW, version 4.3.1; Skamarock et al. (2021)), with initial and boundary conditions provided by the NOAA–NCEP Global Ensemble Forecast System (Hamill et al., 2022). For microphysics, we use the two-moment scheme of Thompson and Eidhammer (2014), which is fully coupled to the Rapid Radiative Transfer Model for GCMs (RRTMG; Iacono et al. (2008)). The simulations are performed on a vertical grid with 55 levels, and the analysis are based on output from the 3-km inner nest. Additional details on model configuration and parameter settings are provided in supporting information of Luschen and Ruppert (2024) and Luschen et al. (2026). A further novelty of this work is that the analysis focuses on the early developmental stage, prior to the time that the storms attained Category 1 intensity. Further details are provided by Luschen et al. (2026).

Tracking of the TC center follows an approach similar to Bourdin et al. (2022), in which the storm center is identified based on vorticity maxima across multiple vertical levels. While this method improves the representation of the track, it fails for 2 and 3 out of the 10 ensemble members of Haiyan and Maria, respectively, as tracking weak vortices remains challenging. These members are therefore excluded from subsequent analyses. Further details are provided in the SI.

2.2. Diurnal Pulses (DPs) in the Simulations

2.2.1. Definition and Identification of DP Signals

A DP event is defined as a continuous outward propagation of grid points exhibiting significant cooling that satisfies the criteria of X. Zhang et al. (2023), including the 25th percentile threshold for brightness temperature anomalies, a minimum duration of 6 hr, and a propagation distance of at least 300 km. Following a similar method to J. Zhang and Du (2025), brightness temperature anomalies are calculated as deviations from a 24-hr triangular-weighted moving average. Figure S3 in Supporting Information S1 presents an example of DP detection for three

10.1029/2026GL123624

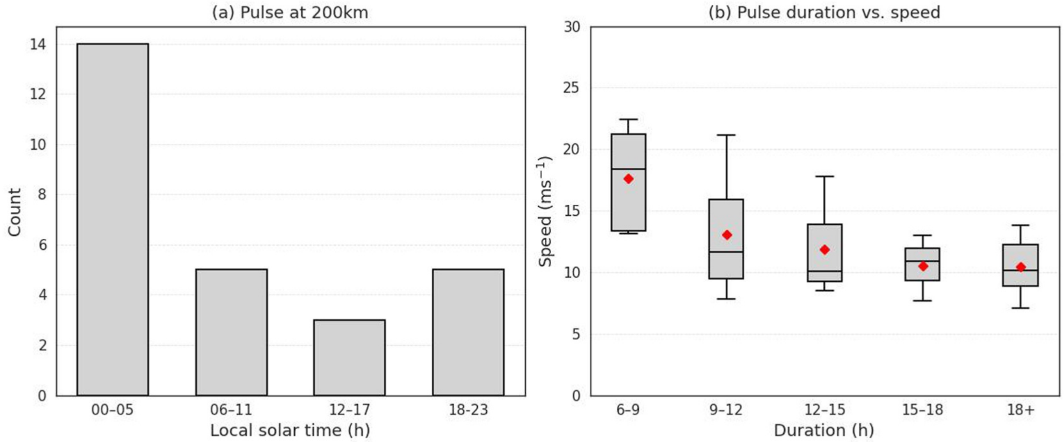

Figure 1. (a) Distribution of LST at which DPs were detected at a 200 km radius. (b) DP propagation speed (ms^{-1}) as a function of DP duration (h). The *x*-axis begins at the threshold for DP classification. Mean values are indicated by red diamonds.

ensemble members of Haiyan, illustrating the methodology and the range of variability across members. For all subsequent analyses, we use hourly model output transformed into cylindrical coordinates centered on the TC tracks. Within this method, DPs are treated as symmetric rings propagating outward from the TC center. Sensitivity to asymmetric structures has not been examined and may introduce a bias in this study. Speed is calculated from the best-fit line fitted to all features that satisfy the DP criteria. Duration is defined as the time from the start to the end of the fitted line.

2.2.2. Characteristics of Simulated DPs

Model performance and suitability for studying DPs are assessed by comparing the frequency, propagation speed, duration, and occurrence time of simulated DPs with observations. All reliable model members exhibit at least one DP, consistent with the results of Ditchek et al. (2019), who showed that such DPs are common even in weak TCs. Figure 1a shows the LST of both TCs when DPs were detected at a 200 km radius. Roughly half of the DPs occur between night and early morning (00–05 LST), with the remainder distributed across other times of day. This overall tendency for detections from early night through the morning hours roughly matches the "Dunion clock" and is consistent with previous findings (Dunion et al., 2014; X. Zhang et al., 2023).

Figure 1b shows the distribution of DP propagation speeds as a function of duration, which is consistent with previous observational results (X. Zhang et al., 2023). For longer-duration DPs, propagation speeds tend to level off around 10–12 m s^{-1}, in agreement with earlier measurements (Ditchek et al., 2019; Dunion et al., 2014; X. Zhang et al., 2023).

3. Evaluation of TC Structure During DP Events

Our analysis in this and the following sections focuses on Super Typhoon Haiyan. Simulations of Hurricane Maria showed substantially delayed intensification for reasons that remain unclear, with weaker signatures of DP amplitudes and fewer DPs overall compared to the Haiyan simulations. Nevertheless, we still performed the analyses for Maria, and obtained consistent results (Figures S5–S7 in Supporting Information S1).

Figure 2 highlights the coherent anomaly patterns associated with DPs propagating through the TC. By construction, T'_B exhibits a pronounced minimum at the DP location. P' reaches its maximum slightly radially inward of the T'_B minimum, indicating a radial and temporal lag between the coldest cloud-tops and peak precipitation (Figure 2a). Enhanced rainfall associated with the DP is defined as P' within 60 km radially inward of the DP, based on this observed lag (see Text S2 in Supporting Information S1). Median values are approximately 4 mm h^{-1} and decrease slightly with radial distance from the TC center. Notably, 90%–95% of DPs show an associated rainfall enhancement, and this fraction increases with increasing radius. These results contrast with those of X. Zhang and Xu (2022)X. Zhang and Xu (2022), who reported cloud–precipitation coupling in only about 50% of

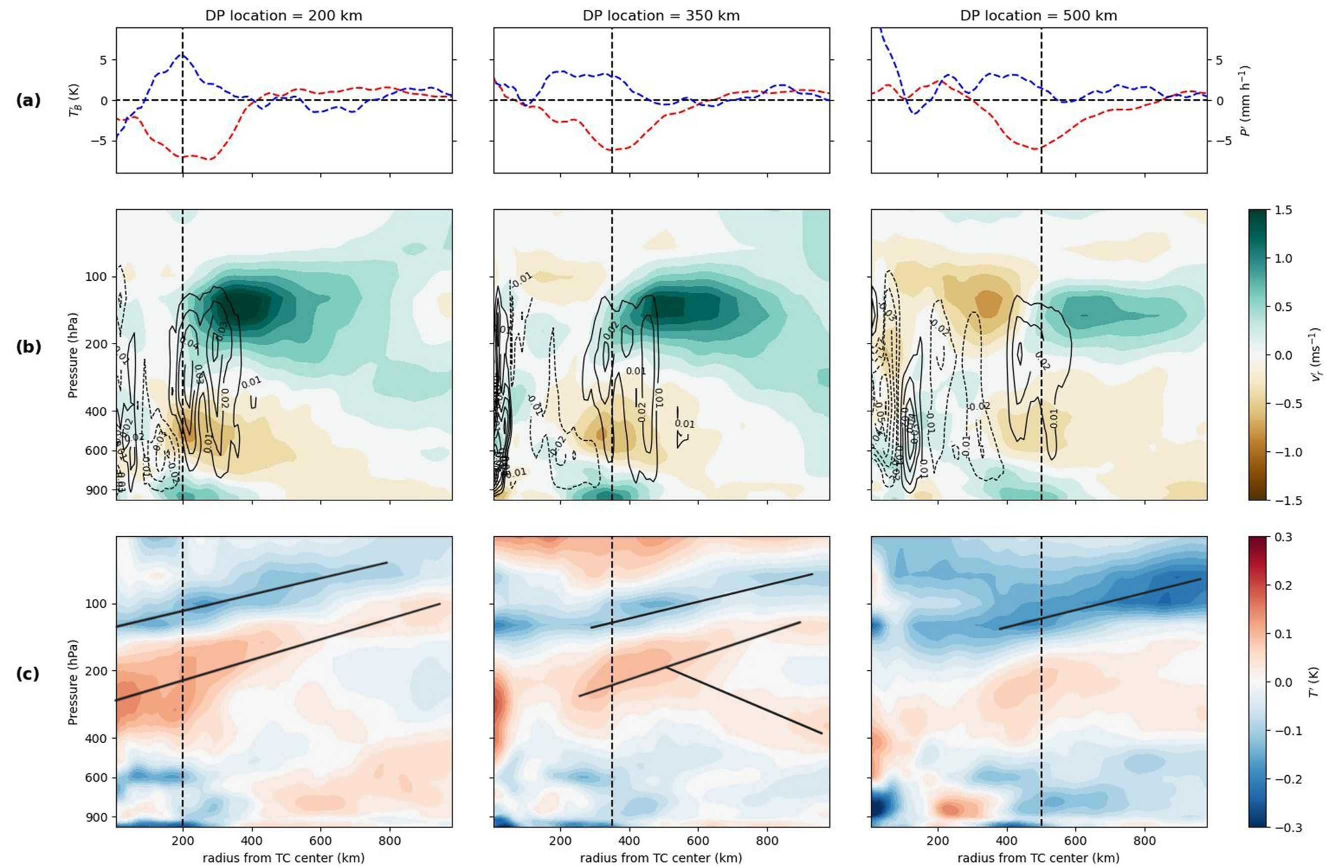

Figure 2. Ensemble-mean composites from Supertyphoon Haiyan showing anomalies associated with DPs detected at radii of 200 km (left), 350 km (center), and 500 km (right) from the TC center. Shown are (a) brightness temperature (T_B'; red) and rainfall (P'; blue) (b) radial wind (v_r'; shading) and vertical velocity (w'; contours: solid/dashed for positive/negative; ms^{-1}) and (c) temperature (T'; shading) anomalies. Solid lines in (c) show propagation angles (see Section 3). All variables are smoothed using a 30-km running window to reduce noise.

cases. The discrepancy likely reflects methodological differences, as we consider all enhanced precipitation near a DP, whereas X. Zhang and Xu (2022) focused on precipitation pulses, employing a method analogous to their brightness temperature DP detection. Their inclusion of higher-shear cases may also weaken the relationship.

Figure 2b further shows a positive w' collocated with and extending slightly ahead of the DP (i.e., radially outward from the TC center), with a trailing negative w'. This structure is consistent with the findings of Dunion et al. (2019), who also documented enhanced upward motion at the DP location. In the upper troposphere, a positive v_r' appears ahead of the DP, accompanied by a negative v_r' in its wake, most prominently at larger radii. At mid-levels, a negative v_r' indicative of enhanced inflow is observed, while near the surface, a positive v_r' consistent with outflow is present. The magnitude of v_r' in the lower and middle levels is comparable to that of the background TC secondary circulation (not shown), therefore DPs can have a substantial impact on inflow. Examination of the T' field (Figure 2c) reveals both upward- and downward-sloping signatures emerging from approximately the 200–300 hPa level indicated by the black solid lines. This level can be interpreted as the approximate location of maximum diabatic heating from which gravity waves are excited. The expected upward and downward energy propagation above and below this level implies downward and upward phase propagation, respectively, consistent with the observed sloped signatures.

4. DP Propagation Mechanism Within Classical Gravity Wave Theory

4.1. Propagation Speed and Angle

Consistent with previous studies (Ditchek et al., 2019; Dunion et al., 2014; X. Zhang et al., 2023), the propagation speeds of longer-duration DPs generally stabilize around 10–12 ms^{-1} (Figure 1), close to the theoretical speeds of gravity waves reported by Navarro and Hakim (2016). The estimated angles of vertical tilt from temperature anomalies (Figure 2c), calculated using the arctangent between the start and end points of each line segment, are in the order of $\pm 1°$ and therefore in line with expectations for gravity waves in a TC environment (O'Neill et al., 2017). These observations indicate that DPs in our study exhibit characteristics similar to those previously associated with gravity-wave–driven phenomena.

4.2. The Construction of the DP Phase Space

To further assess the consistency of the DP structure with gravity waves, we adapt Sakaeda et al. (2020) approach to examine phase relationships among variables by constructing a DP phase space based on brightness temperature anomalies. This approach allows assessment of these relationships regardless of the initiation time or propagation speed of individual DPs.

The DP phase space is constructed using the brightness temperature anomaly (T'_B) and its temporal tendency (dT'_B/dt), both normalized by their respective standard deviations (σ). A phase of $0°/360°$ corresponds to the peak of the warm cloud DP (maximum positive T'_B), while $180°$ represents the center of the cold cloud DP (minimum negative T'_B), and can be interpreted as a normalized time dimension such that phase increases monotonically with time. The amplitude is defined as follows:

$$A = \sqrt{\left(\frac{T'_B}{\sigma_{T'_B}}\right)^2 + \left(\frac{dT'_B/dt}{\sigma_{dT'_B/dt}}\right)^2} \tag{1}$$

Only time steps with amplitude $A > 0.5$ are included in the analysis to ensure focus on significant signals. The DP phase space is divided into 12 bins of $30°$ width each, allowing us to compute statistics of DP characteristics as a function of DP phase.

4.3. Phase Relationships

Gravity waves exhibit characteristic polarization relationships that provide a useful diagnostic for their identification. The following polarization relationships are adapted from established formulations in the literature (Markowski & Richardson, 2011):

$$v'_r = \frac{k_r}{m} w' \tag{2}$$

$$T' = -\frac{i}{\Omega} \frac{N^2 \bar{T}}{g} w' \tag{3}$$

Here, k_r denotes the radial wavenumber, m the vertical wave number, N the Brunt-Väisäla-frequency, g gravitational acceleration, and Ω the intrinsic wave frequency. For gravity waves associated with DPs, a $90°$ phase lag is expected between the temperature anomaly (T') and the vertical velocity anomaly (w'). In addition, the radial wind anomaly (v'_r) is expected to be either in phase with or $180°$ out of phase with w' (Markowski & Richardson, 2011).

Figure 3a shows the expected $90°$ phase lag between w' and T' above 200 hPa and below 400 hPa, which is confirmed by the calculated phase difference in Figure 3d. A notable deviation occurs in the 200–400 hPa layer, where T' and w' are approximately in phase.

Figure 3b shows that v'_r and w' are in phase at upper levels and nearly $180°$ out of phase at lower levels. This transition is confirmed by the calculated phase difference in Figure 3e. Both phase relationships are consistent with linear dry gravity wave theory. However, under uniform propagation conditions, only one of these behaviors would typically be expected rather than both occurring simultaneously. This apparent inconsistency can be explained by differences in the direction of the vertical phase speed, which determines whether the anomalies are in-phase or out-of-phase. In Equation 2, the radial wavenumber k_r is assumed to be positive, corresponding to radially outward propagation. The vertical wave number m is given by

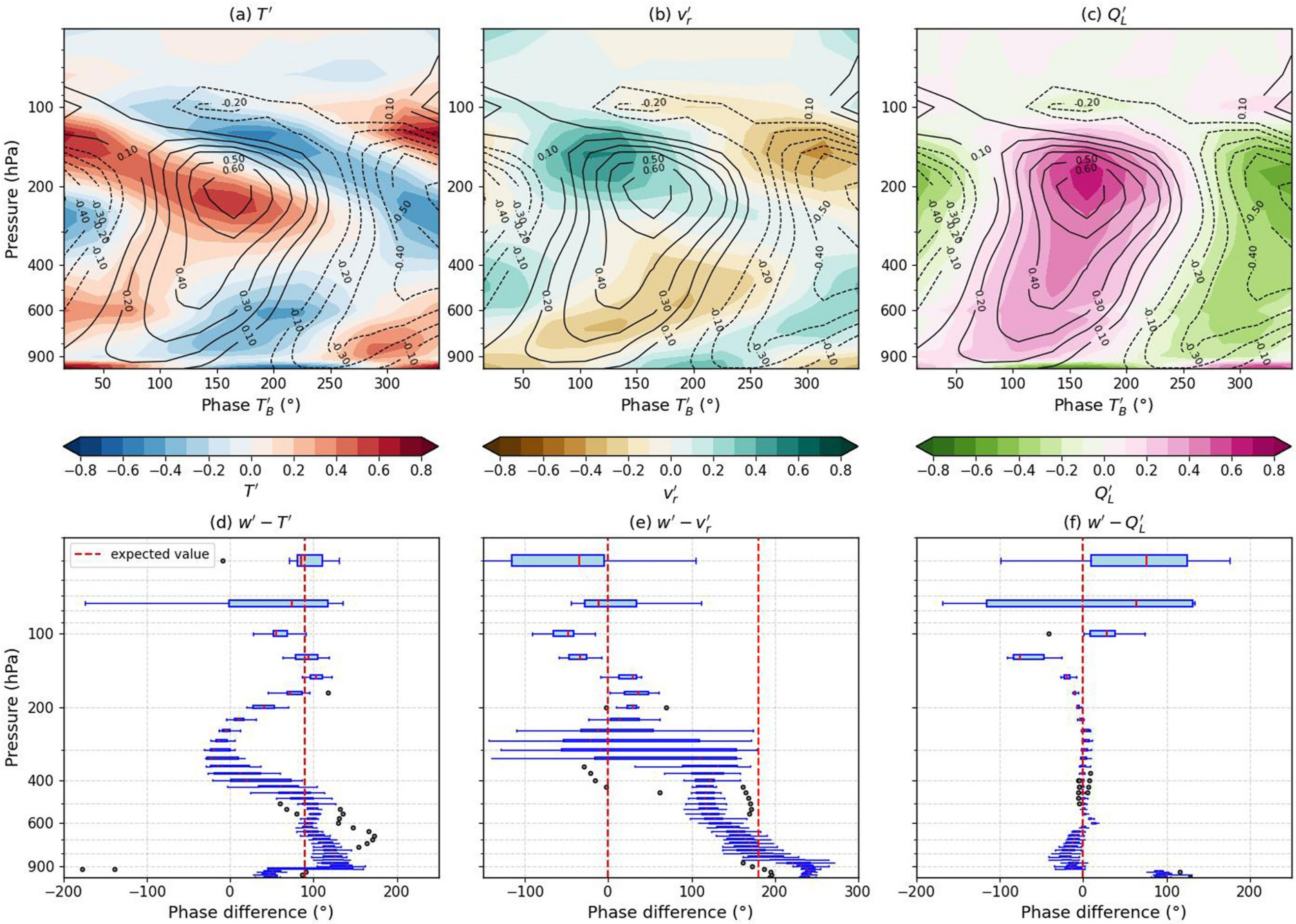

Figure 3. Panels (a–c) present ensemble-averaged anomalies normalized by their standard deviation for Super Typhoon Haiyan averaged over radii of 200–800 km, including (a) temperature anomaly T', (b) radial wind anomaly v_r', and (c) latent heating anomaly Q', as a function of the DP phase space (°). Shading shows each variable, while contours indicate vertical velocity anomalies w' (solid: positive, dashed: negative). Panels (d–f) show the corresponding phase differences relative to w'. Red lines within the boxes indicate the median value across all ensemble members, and the red dashed line denotes the expected phase difference for the respective variable.

$$m = \frac{2\pi}{c_{pz} \cdot \tau} \tag{4}$$

where c_{pz} denotes the vertical phase speed and τ the wave period, which is always positive. We find positive and negative vertical phase speeds (c_{pz}) in the lower and upper troposphere, respectively, which are evident in the positive and negative tilts of radial wind anomalies in the lower and upper troposphere, respectively (see Figure S4 in Supporting Information S1 and Figure 6 in O'Neill et al. (2017)). This explains the observed sign change in the phase relationship between v_r' and w'.

Figure 3c shows that Q' and w' are mostly in phase, as confirmed in Figure 3f, and peak Q' near 200 hPa.

4.4. Effects of Latent Heating on DPs

As discussed in Section 4.3, the middle troposphere (approximately 200–400 hPa) does not exhibit the phase relationships between T' and w' expected for dry gravity waves. One possible explanation is the presence of peak latent heating (Q') in this layer (Figure 3c), which influences temperature. There is also a close alignment between the structure of Q' and w' as discussed previously. This provides a physical explanation for the deviation from the expected phase relationships: the adiabatic cooling associated with ascending motion is partially offset by latent heating from convection, reducing and shifting the net T' and thereby altering the phase relationship

10.1029/2026GL123624

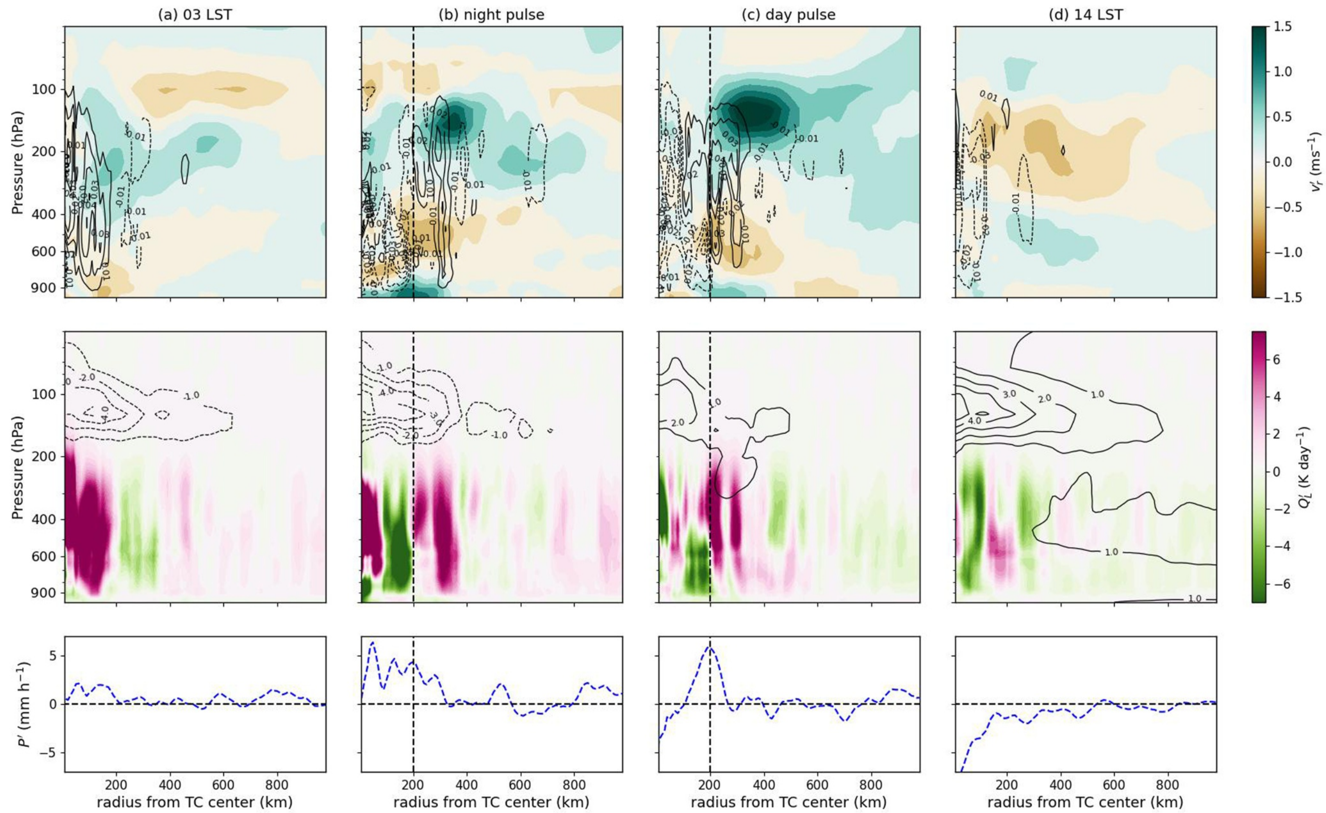

Figure 4. Ensemble-mean composites from Super Typhoon Haiyan showing anomalies associated with (a) 03 LST, (b) night DP (detection at 200 km between 00 and 06 LST), (c) day DP (detection at 200 km after 06 LST) and (d) 14 LST as functions of pressure (hPa) and radius from the TC center (km). Upper panels show radial wind (v_r'; shading) and vertical velocity (w'; contours: solid/dashed for positive/negative; ms^{-1}) anomalies. Middle panels show latent heating (Q_L'; shading) and net radiative tendency (Q_R'; contours: solid/dashed for positive/negative; K day^{-1}). Lower panels show rainfall anomalies (P'; blue). DP occurrences are excluded at 03 LST and 14 LST. All variables are smoothed similar to Figure 2.

between the variables. Similar deviations in the phase relationship between T' and w' are a feature of convectively coupled gravity waves and have been attributed to latent heating (Haertel & Kiladis, 2004; Nakamura & Takayabu, 2022). Furthermore, the structure of Q' and T' closely resembles that reported for convectively coupled gravity waves by Tulich et al. (2007).

The coupling between vertical motion and latent heating has additional important implications. The close alignment of T', w' and Q' maxima indicates energy input at these levels, a pattern also evident in the figures of Evans and Nolan (2019) for energy input through radiative processes. Furthermore, Inoue et al. (2020) argue that this alignment of Q' and T' drives the instability of convectively coupled gravity waves, whereas an out-of-phase relationship would lead to damping. Consequently, energy input from latent heating can help sustain the wave during propagation by reinforcing its ascending branch (warm gets warmer). In this way, the coupling to convection not only explains the altered phase relationships in DPs but also highlights the important role of convection in maintaining the wave as it propagates away from TC center.

5. Preferential Nighttime Occurrence of DPs

Figure 4 illustrates the differences between (b) *night DPs* (detection at 200 km between 00 and 06 LST) and (c) *day DPs* (detection at 200 km after 06 LST). Although the overall structure and outflow patterns are broadly similar, the positive v_r' in daytime DPs occurs at slightly higher altitudes and exhibits a larger peak magnitude. Both DP types are associated with a positive Q_L' ahead of the DP, with the night DP showing a slightly larger magnitude (7.9 Kday^{-1}) compared to the daytime DP (6.2 Kday^{-1}). In terms of P', daytime DPs display a more pronounced P' maximum near the DP location, whereas P' associated with nighttime DPs is more spatially distributed.

When comparing DP-related features to the background diurnal circulation anomalies in TCs, with times of DP occurrence excluded, the DP structure more closely resembles the nocturnal circulation pattern at 03 LST (Figure 4a). All three cases, namely the nocturnal circulation pattern as well as the nighttime and daytime DP (Figures 4a–4c), exhibit a circulation configuration that is favorable for enhanced inner-core convection and is characterized by strengthened low-level inflow and enhanced upper-level outflow. This favorable configuration is reflected in positive Q_L' associated with convection and positive w' in the inner core region. This favorable state for convection is further visible by widespread positive P' during nighttime hours. These findings are consistent with observations of nocturnal maximum rainfall in TCs (Bowman & Fowler, 2015; Dunion et al., 2014; Wu et al., 2015) and with modeling studies linking circulation changes to convection in TCs (Ruppert & O'Neill, 2019). In contrast, convection is suppressed during daytime at 14 LST (Figure 4d), as indicated by negative Q', w' and P', especially in the inner radii (<200 km). Additionally, substantially reduced low-level inflow and its upward shift are less favorable for deep convection and promote dry-air import and ventilation (Ruppert & O'Neill, 2019). The main cause of this suppression and the associated circulation change is the strong shortwave heating of the cirrus canopy (not shown), which also leads to a lifting of the outflow region during daytime (Ruppert & O'Neill, 2019). This lifting may explain the appearance of radial wind anomalies at higher levels during the *day DP* (Figure 4.4b-c; top panel).

As discussed in Section 4.4, we claim that DPs can be interpreted as convectively coupled gravity waves, with convection playing a central role in maintaining them. The results depicted in Figure 4 suggest a positive coupling between DPs and the nocturnal circulation, facilitated by a more favorable environment for deep convection, whereas destructive interference appears to occur during daytime. The constructive nocturnal interference may explain the higher frequency of DPs observed at night compared to daytime.

Regarding the mechanisms responsible for triggering DPs, we hypothesize the existence of two distinct triggering mechanisms depending on the time of initiation (see also Evans and Nolan (2022)). Both mechanisms generate a gravity-wave response associated with DPs. At night, DPs are initiated by convective plumes, as evidenced by enhanced Q_L' and w' and generally stronger convection. Sudden changes in static stability due to such stronger convection would thus excite gravity waves. Consistent with this idea, Ditchek et al. (2019) reported that overnight enhanced deep convection in the inner core was a key precursor to cooling DPs. During the daytime, however, this mechanism appears less likely due to a less favorable environment for convection. Instead, the daytime onset of shortwave heating of the cirrus canopy may act as the dominant triggering mechanism as suggested by Evans and Nolan (2019). Other mechanisms beyond the ones proposed here may also trigger diurnal gravity-wave responses, highlighting the need for further study.

6. Summary and Conclusion

This study has examined the characteristics and underlying mechanisms of diurnal pulses (DPs) using convection-permitting ensemble simulations of two distinct tropical cyclones (TCs). Specifically, we aimed to (a) provide a detailed characterization of the vertical extent of DPs, (b) identify their propagation mechanism, and (c) examine the processes responsible for their preferential nighttime initiation.

Analysis of the TC structure during DP events indicates that DPs are associated with enhanced upper-level outflow radially outward of the DP, while anomalously weaker outflow inside the DP is only evident when the DP is located farther from the TC center. DPs are also associated with substantially reduced low-level inflow and enhanced midlevel inflow near the DP location. They are further associated with positive vertical velocity at and ahead of the DP position, as well as increased precipitation in its wake. Temperature anomalies exhibit upward- and downward-sloping structures associated with the expected dispersion of wave energy (group velocity), propagating upward above and downward below the approximate level of the heat source. All anomalies display organized vertical and radial patterns that evolve systematically as the DP propagates through the TC.

An examination of propagation speeds, propagation angles, and, most notably, the phase relationships among the various variables within a classical dry gravity wave framework provides strong support for gravity wave propagation as the mechanism governing DP propagation. However, departures from the expected phase relationships in the 200–400 hPa layer require further explanation. We provide evidence that these deviations are attributable to interactions with convection and latent heat release, given strong consistency with convectively coupled gravity waves (Haertel & Kiladis, 2004; Tulich et al., 2007). Furthermore, the alignment of latent heating with positive temperature anomalies underscores the importance of moist convection for sustaining the DP-associated wave by driving its instability (Inoue et al., 2020).

The composite DP structure more closely resembles the nocturnal part of the diurnally varying transverse circulation of the TC, characterized by enhanced low-level inflow and upper-level outflow that favor convective development in the inner core (Ruppert & O'Neill, 2019). This background nocturnal circulation constructively interferes with the DP-induced anomalies, potentially explaining the preferential nocturnal initiation of DPs. In contrast, during daytime hours, reversal of these transverse circulation anomalies favor the suppression of convection, which is destructive for DP signals.

Based on these results, we hypothesize the existence of two distinct initiation mechanisms for DPs. During nighttime, enhanced inner-core convection or convective plumes associated with radiative destabilization, particularly in the upper troposphere above 200 hPa, may perturb static stability and generate a gravity wave response. During daytime, shortwave solar heating of the cloud canopy may act as an alternative triggering mechanism (Evans & Nolan, 2019). Future studies are needed to further evaluate and quantify these proposed initiation pathways.

Conflict of Interest

The authors declare no conflicts of interest relevant to this study.

Availability Statement

The data and code for the analysis and the plots included in this paper are published on Zenodo (Schmitt et al., 2026).

Acknowledgments
Support for this work has been provided by the National Science Foundation under Grant AGS-2331120, the Deutsche Forschungsgemeinschaft (DFG, German Research Foundation) under *Germany's Excellence Strategy—EXC 2037* "*Climate, Climatic Change, and Society*" (project number 390683824), and the European Research Council through the ERC starting grant ROTOR (Grant 101116282). Open Access funding enabled and organized by Projekt DEAL.

References

Bourdin, S., Fromang, S., Dulac, W., Cattiaux, J., & Chauvin, F. (2022). Intercomparison of four algorithms for detecting tropical cyclones using ERA5. *Geoscientific Model Development*, *15*(17), 6759–6786. https://doi.org/10.5194/gmd-15-6759-2022

Bowman, K. P., & Fowler, M. D. (2015). The diurnal cycle of precipitation in tropical cyclones. *Journal of Climate*.

Cangialosi, J. P., Blake, E., DeMaria, M., Penny, A., Latto, A., Rappaport, E., & Tallapragada, V. (2020). Recent progress in tropical cyclone intensity forecasting at the national hurricane center. *Weather and Forecasting*, *35*(5), 1913–1922. https://doi.org/10.1175/WAF-D-20-0059.1

Ditchek, S. D., Corbosiero, K. L., Fovell, R. G., & Molinari, J. (2020). Electrically active diurnal pulses in Hurricane Harvey (2017). *Monthly Weather Review*, *148*(6), 2283–2305. https://doi.org/10.1175/MWR-D-20-0022.1

Ditchek, S. D., Molinari, J., Corbosiero, K. L., & Fovell, R. G. (2019). An objective climatology of tropical cyclone diurnal pulses in the Atlantic Basin. *Monthly Weather Review*, *147*(2), 591–605. https://doi.org/10.1175/MWR-D-18-0368.1

Dunion, J. P., Thorncroft, C. D., & Nolan, D. S. (2019). Tropical cyclone diurnal cycle signals in a hurricane nature run. *Monthly Weather Review*, *147*(1), 363–388. https://doi.org/10.1175/MWR-D-18-0130.1

Dunion, J. P., Thorncroft, C. D., & Velden, C. S. (2014). The tropical cyclone diurnal cycle of mature hurricanes. *Monthly Weather Review*, *142*(10), 3900–3919. https://doi.org/10.1175/MWR-D-13-00191.1

Evans, R. C., & Nolan, D. S. (2019). Balanced and radiating wave responses to diurnal heating in tropical cyclone–like vortices using a linear nonhydrostatic model. *Journal of the Atmospheric Sciences*, *76*(8), 2575–2597. https://doi.org/10.1175/JAS-D-18-0361.1

Evans, R. C., & Nolan, D. S. (2022). The spatiotemporal evolution of the diurnal cycle in two WRF simulations of tropical cyclones. *Journal of the Atmospheric Sciences*, *79*(4), 1021–1043. https://doi.org/10.1175/JAS-D-21-0100.1

Haertel, P. T., & Kiladis, G. N. (2004). Dynamics of 2-day equatorial waves. *Journal of the Atmospheric Sciences*, *61*(22), 2707–2721. https://doi.org/10.1175/JAS3352.1

Hamill, T. M., Whitaker, J. S., Shlyaeva, A., Bates, G., Fredrick, S., Pegion, P., et al. (2022). The reanalysis for the global ensemble forecast system, version 12. *Monthly Weather Review*, *150*(1), 59–79. https://doi.org/10.1175/MWR-D-21-0023.1

Iacono, M. J., Delamere, J. S., Mlawer, E. J., Shephard, M. W., Clough, S. A., & Collins, W. D. (2008). Radiative forcing by long–lived greenhouse gases: Calculations with the AER radiative transfer models. *Journal of Geophysical Research*, *113*(D13). https://doi.org/10.1029/2008JD009944

Inoue, K., Adames, Á. F., & Yasunaga, K. (2020). Vertical velocity profiles in convectively coupled equatorial waves and MJO: New diagnoses of vertical velocity profiles in the wavenumber–frequency domain. *Journal of the Atmospheric Sciences*, *77*(6), 2139–2162. https://doi.org/10.1175/JAS-D-19-0209.1

Kaplan, J., DeMaria, M., & Knaff, J. A. (2010). A revised tropical cyclone rapid intensification index for the Atlantic and eastern North Pacific basins. *Weather and Forecasting*, *25*(1), 220–241. https://doi.org/10.1175/2009WAF2222280.1

Luschen, E., Ruppert, J., Rios-Berrios, R., Wu, S.-N., & Zhang, Y. (2026). Stratiform and anvil cloud–radiative forcing in tropical cyclogenesis. *Geophysical Research Letters*, *53*(1), e2025GL119765. https://doi.org/10.1029/2025GL119765

Luschen, E., & Ruppert, J. H. (2024). Longwave radiative feedback due to stratiform and anvil clouds. *Geophysical Research Letters*, *51*, e2024GL108668. https://doi.org/10.1029/2024GL108668

Markowski, P., & Richardson, Y. (2011). *Mesoscale meteorology in midlatitudes*. Wiley-Blackwell. https://doi.org/10.1002/9780470682104

Nakamura, Y., & Takayabu, Y. N. (2022). Convective couplings with equatorial Rossby waves and equatorial kelvin waves. Part I: Coupled wave structures. *Journal of the Atmospheric Sciences*, *79*(1), 247–262. https://doi.org/10.1175/JAS-D-21-0080.1

Navarro, E. L., & Hakim, G. J. (2016). Idealized numerical modeling of the diurnal cycle of tropical cyclones. *Journal of the Atmospheric Sciences*, *73*(10), 4189–4201. https://doi.org/10.1175/JAS-D-15-0349.1

O'Neill, M. E., Perez-Betancourt, D., & Wing, A. A. (2017). Accessible environments for diurnal-period waves in simulated tropical cyclones. *Journal of the Atmospheric Sciences*, *74*(8), 2489–2502. https://doi.org/10.1175/JAS-D-16-0294.1

Razin, M. N., Slocum, C. J., Knaff, J. A., & Brown, P. J. (2023a). *Tropical cyclone precipitation, infrared, microwave, and environmental dataset (tc primed)*. NOAA National Centers for Environmental Information. https://doi.org/10.25921/DMY1-0595

Razin, M. N., Slocum, C. J., Knaff, J. A., Brown, P. J., & Bell, M. M. (2023b). Tropical cyclone precipitation, infrared, microwave, and environmental dataset (tc primed). *Bulletin of the American Meteorological Society*, *104*(11), E1980–E1998. https://doi.org/10.1175/BAMS-D-21-0052.1

Ruppert, J. H., & O'Neill, M. E. (2019). Diurnal cloud and circulation changes in simulated tropical cyclones. *Geophysical Research Letters*, *46*(1), 502–511. https://doi.org/10.1029/2018GL081302

Ruppert, J. H., Wing, A. A., Tang, X., & Duran, E. L. (2020). The critical role of cloud-infrared radiation feedback in tropical cyclone development. *Proceedings of the National Academy of Sciences of the United States of America*, *117*(45), 27884–27892. https://doi.org/10.1073/pnas.2013584117

Sakaeda, N., Kiladis, G., & Dias, J. (2020). The diurnal cycle of rainfall and the convectively coupled equatorial waves over the maritime continent. *Journal of Climate*, *33*(8), 3307–3331. https://doi.org/10.1175/JCLI-D-19-0043.1

Schmitt, K., Ruppert, J., Sakaeda, N., & Vogel, R. (2026). Data for diurnal pulses in tropical cyclones as convectively coupled gravity waves (v1.0.0). https://doi.org/10.5281/zenodo.20810819

Shimada, U., Owada, H., Yamaguchi, M., Iriguchi, T., Sawada, M., Aonashi, K., et al. (2018). Further improvements to the statistical hurricane intensity prediction scheme using tropical cyclone rainfall and structural features. *Weather and Forecasting*, *33*(6), 1587–1603. https://doi.org/10.1175/WAF-D-18-0021.1

Skamarock, W. C., Ong, H., & Klemp, J. B. (2021). A fully compressible nonhydrostatic deep-atmosphere equations solver for MPAS. *Monthly Weather Review*, *149*(2), 571–583. https://doi.org/10.1175/MWR-D-20-0286.1

Thompson, G., & Eidhammer, T. (2014). A study of aerosol impacts on clouds and precipitation development in a large winter cyclone. *Journal of the Atmospheric Sciences*, *71*(10), 3636–3658. https://doi.org/10.1175/JAS-D-13-0305.1

Trabing, B. C., & Bell, M. M. (2021). Observations of diurnal variability under the cirrus canopy of Typhoon Kong-Rey (2018). *Monthly Weather Review*. https://doi.org/10.1175/MWR-D-20-0327.1

Tulich, S. N., Randall, D. A., & Mapes, B. E. (2007). Vertical-mode and cloud decomposition of large-scale convectively coupled gravity waves in a two-dimensional cloud-resolving model. *Journal of the Atmospheric Sciences*, *64*(4), 1210–1229. https://doi.org/10.1175/JAS3884.1

Wu, Q., Ruan, Z., Chen, D., & Lian, T. (2015). Diurnal variations of tropical cyclone precipitation in the inner and outer rainbands. *Journal of Geophysical Research: Atmospheres*, *120*(1), 1–11. https://doi.org/10.1002/2014JD022190

Zhang, J., & Du, Y. (2025). Revisiting the diurnal pulses of tropical cyclones over the northwest Pacific Ocean. *Geophysical Research Letters*, *52*(14), e2025GL116554. https://doi.org/10.1029/2025GL116554

Zhang, X., Ditchek, S. D., Corbosiero, K. L., & Xu, W. (2023). Global and regional characteristics of radially outward propagating tropical cyclone diurnal pulses. *Journal of Geophysical Research: Atmospheres*, *128*(7), e2022JD037660. https://doi.org/10.1029/2022JD037660

Zhang, X., & Xu, W. (2021). Strong diurnal pulsing of cold clouds in rapidly intensifying tropical cyclones. *Geophysical Research Letters*, *48*(21), e2021GL094773. https://doi.org/10.1029/2021GL094773

Zhang, X., & Xu, W. (2022). Is there an outward propagating diurnal signal in the precipitation of tropical cyclones? *Geophysical Research Letters*, *49*(4), e2021GL097166. https://doi.org/10.1029/2021GL097166

Zhang, X., Zhuo, J.-Y., Bao, X., Tan, Z.-M., Guo, S., & Zhu, K. (2026). Integrating diurnal pulsing signatures for AI–driven tropical cyclone intensity prediction. *Geophysical Research Letters*, *53*(4), e2025GL119496. https://doi.org/10.1029/2025GL119496